Signatures of ring currents in a magnetic mirror plasma experiment

Signatures of Ring Currents in a Magnetic Mirror Plasma Experiment.

P.J. Mc Carthy and S. Knott

Department of Physics, University College Cork, Cork, Ireland

E-mail: pjm@ucc.ie

Abstract.
Spatial profiles of electron density and temperature obtained from Langmuir probe data in a magnetic mirror plasma experiment using permanent rare-earth magnet stacks show clear signatures of azimuthal or ring currents generated by grad B and curvature drifts. The plasma-generating hot cathode filament is placed within the mirror so that the primary electrons generated with energies $\simeq 75$ eV are confined by the magnetic mirror effect resulting in a combination of a rapid bounce motion with a slower azimuthal drift whose direction is determined by the orientation of the magnet stacks. A spatial scan using a movable Langmuir probe system shows two peaks of unequal amplitude in the hot electron density profile at locations along the probe path corresponding to $\phi = 90°$ and $\phi = 270°$ where the filament is located at $\phi = 0$. The position of the stronger peak is consistent with the shorter path in the electron drift direction for the choice of orientation of the magnets. Reversing the magnetic orientation exchanges the locations of the strong and weak hot electron density peaks. The dependence of the ratio of the two peak amplitudes on gas pressure p is consistent with exponential attenuation of the hot electron density along the drift orbit with a mean free path $\lambda_{mfp} \propto 1/p$.

(Figures in this article are in colour only in the electronic version)

1. Introduction

Azimuthal or ring currents primarily consisting of energetic ions play a central role in the geophysics of the earth's magnetosphere, in particular in the reduction in the terrestrial magnetic field strength due to their intensification during geomagnetic storms [1, 2]. They were first postulated by Chapman and Ferraro in 1931 [3] and first experimentally confirmed by spacecraft measurements starting with *Explorer VI* [4]. Although recent work has been done on the detection of azimuthal current flow in plasma accelerators [5, 6], to our knowledge no results of steady state ring current detection in laboratory experiments have been reported previously. Hollow density profiles, a natural outcome of the experiment reported on here, were recently observed in a helicon device [7], but the more complex vessel geometry and magnetic structure in that work made it difficult to draw definitive conclusions on the mechanism underlying their formation. Here, we report results obtained from analysis of Langmuir probe data acquired in a spatial scan through an axisymmetric magnetic mirror plasma which shows clear signatures of ring currents. After a description of the experimental set-up, the data analysis method and a review of some elementary magnetic mirror theory, electron density and temperature profiles are presented for a range of neutral pressures, in each case for two magnetic field orientations, which unambiguously demonstrate the presence of strong azimuthal currents. This is followed by a discussion and some concluding remarks.

2. Experimental Setup

The apparatus used in this research is a Double Plasma device reconfigured as a magnetic mirror experiment. A schematic is shown in figure 1. The cylindrical stainless steel vessel has an internal diameter of 25 cm and a length of 47 cm. To limit the rise in wall temperature for maximum heating powers of several kilowatts the curved cylindrical surface is surrounded by a $\simeq 12$ mm jacket through which cooling water flows. The baseplate of the cylindrical chamber is air-cooled. The magnetic mirror is formed by two stacks of NdFeB rare–earth permanent magnets (internal field = 1.25 T) aligned coaxially and placed diametrically opposite one another against the curved cylinder surface to form an axisymmetric, non-uniform field as shown in figure 1(b). Various stack lengths as well as magnet diameters ranging from 12 mm to 50 mm have been used, but the data presented here were acquired using magnet stacks of length 20 cm and diameter 30 mm. The faces of the magnet stacks are 28.0 cm apart and hence there is a gap of 15 mm between the front face of each stack and the plasma-facing vessel wall. For this configuration, the magnetic field strength along the mirror axis, plotted in figure 1(d), takes a maximum value of 183 mT at the plasma-facing wall surface and a minimum of 5.9 mT at the symmetry plane of the mirror resulting in a mirror ratio of 31 along the mirror axis. The calculated field strength along the mirror axis was experimentally verified with an uncertainty of $\approx \pm 0.2$ mT using a teslameter. As the field line radius in the symmetry plane increases from 0 to 10 cm the mirror ratio

decreases from 31 to 20.

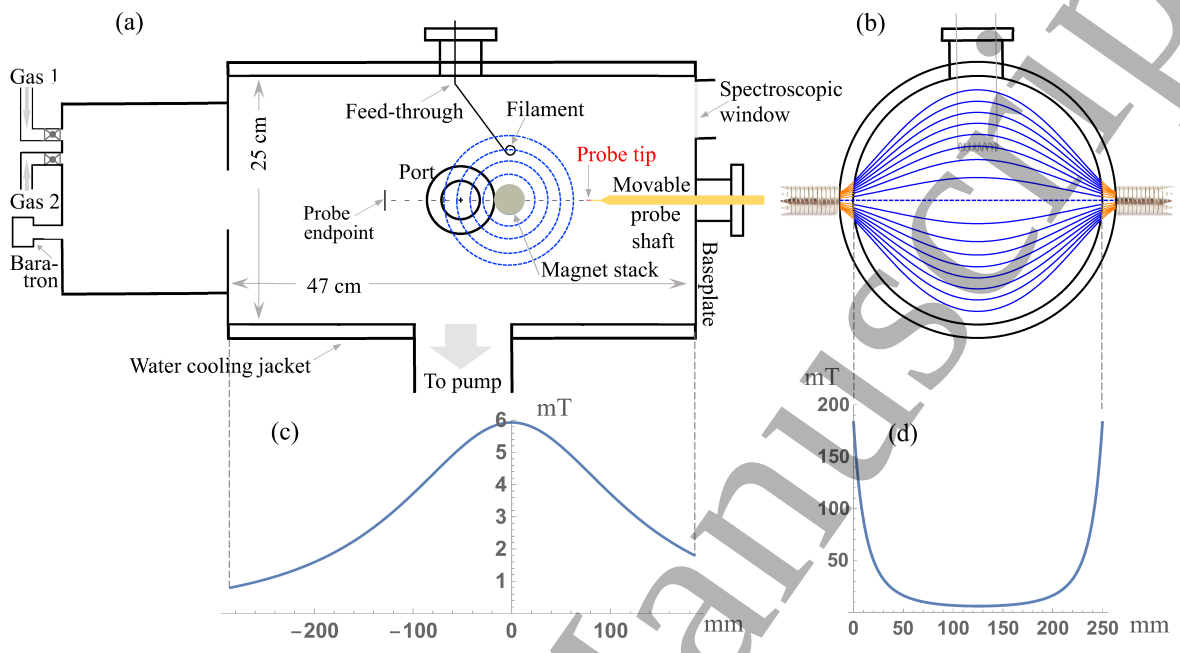

Figure 1. Schematic diagram showing (a) side and (b) end views of the cylindrical vessel with cutaways of the two 20 cm stacks of NeFeB magnets of diameter 3 cm. Magnetic field lines enclosing flux $\phi = \int_0^r \mathbf{B} \cdot d\mathbf{A} =$ 1,3,5,...,15 mWb show the mirror field structure. The orange segments lie within the cooling jacket. The dotted blue line in panel (b) is the mirror axis. The mirror symmetry plane is normal to the axis and equidistant from the two magnet stacks. The magnetic field profile along the vessel axis (coincident with the probe path) is plotted in panel (c), where the zero in the spatial coordinate is in this case located at the position of the mirror axis. The magnetic field profile along the mirror axis is plotted in panel (d).

Two gas inlets are located on the far side of an unused second chamber of rectangular cross-section (see figure 1(a)), and the pumping duct is located midways along the floor of the cylindrical chamber. The outlet is protected by a mesh filter to prevent debris from the filament or probe system damaging the turbo-molecular pump. The cylindrical vessel has three sealed flange ports. One is located at the top of the vessel above the pump and is used for electrical feed-throughs to the filament while the other two face each other horizontally on opposite sides of the vessel. The detachable baseplate of the vessel also has a flange port for the movable Langmuir probe shaft whose 300 mm range, indicated by the dashed line in figure 1(a), coincides with the axis of the cylinder. The baseplate has in addition a spectroscopic window which provides a line of sight perpendicular to the mirror axis. Helium, argon and nitrogen have been used as working gases. The data presented here were acquired in nitrogen plasmas.

Plasmas are generated by thermionic emission of primary electrons from a negatively biased tungsten filament inserted through the top port of the cylindrical chamber. The filament consists of 0.5 mm diameter tungsten wire wound to form a 10 mm diameter coil of geometric length 41 mm and total wire length of 50 cm

manufactured by Plansee GmbH. The coil legs are connected to two molybdenum support rods, which in turn are connected to dual insulated electrical feeds through the vacuum flange. The tungsten coil legs are tightly wound with additional tungsten wire of diameter 0.38 mm to reduce the leg resistance so that incandescence is restricted to the horizontal coil windings. The filament axis is located parallel to and 50 mm above the mirror axis as shown in figure 1. The placing of the filament within the magnetic mirror is a key feature of the experimental set-up, because the primary electrons emitted from the filament are confined within the mirror in a narrow annulus whose initial radial extent in the mirror symmetry plane is $d_{filament} + 2\rho_{gyro} \approx 22$ mm for filament windings of outer diameter 11mm and an electron gyroradius $\rho_{gyro} \approx 5.6$ mm for the experiments reported below where the typical initial primary electron energy was 75 eV in a field of 5.2 mT at the filament location. Furthermore, the excellent fits to Langmuir probe data that are presented in the results section are evidence that the confinement of the primary or hot electron population is long enough to form a good approximation to a Maxwellian distribution of energies, together with a colder population of secondary electrons as assumed by the model which fits the probe data.

Thermionic emission results from Ohmic heating of the tungsten filament, using a Farnell H60/50 power supply, with a threshold power of $\approx$500 W for helium plasmas but which could be as low as $\approx$250 W for nitrogen plasmas. The liberated electrons are accelerated away from the filament with a bias voltage which can range from 35 V to 125 V supplied by a Delta Electronika SM 120-50 power supply which allows for plasma currents of up to 50 A. Inelastic collisions between the energetic primary (hot) electrons and the neutral gas result in two electron populations which requires a bi-Maxwellian model to fit probe data for low gas pressure experiments. The Langmuir probe system used is a modified Impedans Ltd. Langmuir Spatial Probe inserted along the axis of the vessel. The probe tip consists of a tungsten wire of 0.1 mm diameter and exposed length of typically 6 mm attached to the probe cradle which in turn is screwed into a metal probe arm enclosed within a solid ceramic shaft which insulates it from the plasma. To minimise disturbance of the probe measurement by the ceramic cone from which the probe wire tip is designed to protrude, we inserted a length of thin ceramic tubing of inner diameter 0.3 mm and outer diameter 0.7 mm into the 1mm duct through the cone (see figure 1(a)) in keeping with optimal probe design practice [8]. The convenience of the removable ceramic cone was offset by a surface alignment gap of up to 0.2 mm between the cone base and the shaft when the cone was fully screwed in. We attributed frequent distortions of the ion branch of the Langmuir characteristic to the beam-like nature of the ring current [9] which caused ions to penetrate the gap, thus spuriously enhancing the recorded current. The problem disappeared after covering the gap with a 2 mm - thick tightly fitting ceramic collar designed for this purpose by Krosaki Harima Corp. The data presented below for spatial scans covering the 300 mm range of the probe for both magnetic field orientations includes unavoidable perturbations caused by the probe shaft passing through the plasma.

The Langmuir data analysis code, developed by the first author, has already been

described [10]. Note that since the *minimum* magnetic field value of B = 5.9 mT along the mirror axis corresponds to the *maximum* value of B along the spatial scan path of the probe (see subfigures 1(c) and 1(d)), the electron gyroradius satisfies $\rho_e \geq 0.40\sqrt{T_e}$ mm (T_e in eV) which for the temperatures reported here of $T_e > 1$ eV exceeds by a factor of 8 or more the probe radius $r_P = 0.05$ mm and hence magnetization effects can be neglected in the probe analysis [11].

3. Theory

The motion of electrons trapped in an axisymmetric mirror configuration, before collisions are taken into account, consists of a rapid bounce motion along magnetic field lines due to adiabatic conservation of the magnetic moment $\mu = mv_\perp^2/2B$ combined with a slower azimuthal motion resulting from $\nabla_\perp B$ and field line curvature drifts. The bounce period T_{bounce} (the round trip time) for particles near the mirror axis is given by

$$T_{bounce} = 4\int_0^{z_m} \frac{dz}{v_\parallel} \tag{1}$$

where $z = 0$ corresponds to the symmetry plane. Conservation of μ and particle energy $mv^2/2$ (in a region with negligible $E_\parallel$) results in the following expression for $v_\parallel$:

$$v_\parallel = v\sqrt{1 - \frac{B}{B_m}} \tag{2}$$

for a particle trajectory where B takes its maximum value B_m at the two mirror points of the trajectory $z = \pm z_m$. The value of B_m or z_m for a particular particle is determined by its pitch angle $\phi = \arctan v_\perp/v_\parallel$ in the symmetry plane where B takes its minimum value for the trajectory. The field of a uniformly magnetized cylindrical bar magnet can be accurately approximated by that of an idealized finite solenoid, i.e. one with with strictly azimuthal current [12]. Accordingly, the calculation of the magnetic field of the permanent magnet stacks, assumed to be uniformly magnetized, is based on the field of a thin circular current loop. This is given in terms of elliptic functions requiring numerical evaluation, except for the field along the axis of the current loop which, for a loop of radius a carrying a current I, is given by the well-known expression

$$B_{axis}^{current\ loop}(z) = \frac{\mu_0 I a^2}{2(a^2+z^2)^{3/2}} \tag{3}$$

Replacing the loop current I by the current per unit length i (the NdFeB internal field of 1.25 T equates to $i = 0.995\,\mathrm{MA\,m^{-1}}$) and with z replaced by $z + x$, equation (3) is integrated over the range $0 \leq x \leq L$ to yield the axial field for a finite solenoid of length L and radius a with the origin $z = 0$ at the leading end:

$$B_{axis}^{solenoid}(z) = \frac{\mu_0 i}{2}\left(\frac{L+z}{\sqrt{a^2+(L+z)^2}} - \frac{z}{\sqrt{a^2+z^2}}\right) \tag{4}$$

The mirror configuration consists of two coaxial magnet stacks spaced a distance d apart with the symmetry plane a distance $d/2$ from each stack face. The combined axial field

for the two stacks, this time with the origin $z = 0$ in the symmetry plane, is given by

$$B_{axis}^{mirror}(z) = \frac{\mu_0 i}{2}\left(\frac{L+\frac{d}{2}+z}{\sqrt{a^2+(L+\frac{d}{2}+z)^2}} - \frac{\frac{d}{2}+z}{\sqrt{a^2+(\frac{d}{2}+z)^2}} + \right. \\ \left. + \frac{L+\frac{d}{2}-z}{\sqrt{a^2+(L+\frac{d}{2}-z)^2}} - \frac{\frac{d}{2}-z}{\sqrt{a^2+(\frac{d}{2}-z)^2}}\right) \quad (5)$$

Substitution of equation (5) into equation (2) followed by evaluation of equation (1) using the parameters of the experiment ($a = 15\,\text{mm}$, $d = 28\,\text{cm}$, $L = 20\,\text{cm}$) yields a bounce time in microseconds of

$$T_{bounce}\,(\mu s) \approx 1.25\sqrt{\frac{m_j}{T_j}} \quad (6)$$

where T_j is the temperature of plasma species j in electron volts and the particle mass m_j is in units of the electron mass. The approximate nature of the result reflects the fact that there is a modest variation of $\pm 10\%$ in the value of T_{bounce} over the full z_m range: $0 < z_m < 12.5\,\text{cm}$, or equivalently over the full B_m range: $5.9\,\text{mT} < B_m < 183\,\text{mT}$ in the case of the magnetic field value B_m at the mirror points. For the temperatures reported in the next section, electron bounce times lie in the range $0.2\,\mu\text{s} < T_{bounce} < 1.25\,\mu\text{s}$ while singly ionized nitrogen ions have bounce times of order 1 ms.

Ring currents arise from particle drift velocities generated by (i) $\nabla_\perp B$, the perpendicular component of the gradient of the field strength B and (ii) the field line radius of curvature R_c. When plasma pressure is very weak relative to magnetic field pressure $B^2/2\mu_0$, the expressions for both drift velocities have the same dependence on $\mathbf{B}$ and ∇B and both terms combine to give (see, e.g., [13], Chapter 3):

$$\mathbf{v}_{\nabla_\perp B} + \mathbf{v}_{curv.} = \frac{T_\perp + T_\parallel}{q}\frac{\mathbf{B}\times\nabla B}{B^3} \quad (7)$$

In an axisymmetric field this charge-dependent (but mass-independent) drift is strictly azimuthal and furthermore is reversed for all charge species if the magnetic field direction is reversed. Since the filament axis is centred on the symmetry plane and aligned to the local magnetic field direction (see figure 1(b)), the primary electrons will be preferentially emitted normal to the local magnetic field and hence will initially have pitch angles resulting in trajectories confined closer to the symmetry plane than in the case of isotropically emitted primary electrons. To a good approximation, these electrons have a drift speed $v_{dr}(r)$ dependent only on the radius r in the symmetry plane of the flux surface on which they reside. The time taken to complete a drift orbit under these conditions is simply $\mathrm{T}_{orbit} = 2\pi r/v_{dr}(r)$. Taylor expansions at small radii for B and ∇B in the symmetry plane yield $B = a - br^2 + \cdots$ and $\nabla B = -2br\,\hat{\mathbf{r}} + \cdots$ where a and b are positive coefficients. If we assume, at a modest cost in accuracy, a single effective temperature $T \equiv (T_\perp + T_\parallel)/2$ in equation (7), the drift velocity for $\mathbf{B}$ in the positive $\hat{\mathbf{z}}$ direction is given by:

$$\mathbf{v}_{dr} = \frac{2T}{q}\frac{\mathbf{B}\times\nabla B}{B^3}$$

$$= \frac{2T}{q}\frac{(a + b\,r^2 + \cdots)\hat{\mathbf{z}} \times (-2b\,r + \cdots)\hat{\mathbf{r}}}{a^3 - 3a^2 b\,r^2 + \cdots}$$
$$= -\frac{4Tbr}{qa^2}\hat{\boldsymbol{\phi}} + \cdots \tag{8}$$

so that the drift orbit period $\mathrm{T}_{orbit} \propto r/v_{dr}$ is to leading order independent of radius. The drift orbit period for the magnetic field geometry of the experiment for singly charged species was found to be

$$T_{orbit,\,j}(\mu\mathrm{s}) \approx \frac{150}{T_j} \tag{9}$$

for species j where T is in eV and the approximation again indicates variations of $\approx 10\%$ over the radial range $0 < r < 12.5\,\mathrm{cm}$. The quotient of this expression and equation (6) yields the dimensionless ratio (with T in eV and m in units of electron mass)

$$\frac{T_{orbit,\,j}}{T_{bounce,\,j}} \approx \frac{120}{\sqrt{m_j T_j}} \tag{10}$$

This ratio is 120 for 1 eV electrons and 19 for 40 eV electrons which equates to the largest fitted temperatures in the experimental results presented later. By contrast, the ratio for 0.1 eV singly ionized nitrogen ions is 2.4 and hence the bounce motion and drift orbit periods for ions, in contrast to electrons, are comparable. (Measurements of ion temperature in this device for a wide range of plasma parameters in helium plasmas using a FTIR-based high resolution spectrometer yielded a temperature range of $0.08\,\mathrm{eV} < T_i < 0.35\,\mathrm{eV}$ [14] and we use a reference $T_i = 0.1\,\mathrm{eV}$ here.)

If the z axis coincides with the mirror axis and the positive z direction is into the page in figure 1(a), the direction of increasing azimuthal angle $\hat{\boldsymbol{\phi}} = \hat{\mathbf{z}} \times \hat{\mathbf{r}}$ in a right-handed system of cylindrical coordinates is clockwise. From the final expression in equation (8), the drift direction for electrons when the magnetic field is oriented in the positive z direction is in the positive $\hat{\boldsymbol{\phi}}$ direction and is hence also clockwise with reference to figure 1(a). Thus the signature of ring currents for this 'positive' orientation labelled as '**S**' in the next section, should include the following properties:

(i) If y_0 is the position along the probe path directly under the filament which is at a height h ($= 50\,\mathrm{mm}$) above the vessel axis, then a strong local maximum in the hot electron density is expected at a location $y = y_0 - h$, i.e. on the near side (with respect to the baseplate) of the filament where the primary electrons consist of those which have completed a minimum of a quarter of a drift orbit and, for sufficiently low pressure allowing multiple passes, with further contributions from primary electrons that have completed $N + \frac{1}{4}$ drift orbits where $N \geq 1$.

(ii) A weaker local maximum is expected at a location $y = y_0 + h$ on the far side of the filament due to pressure-dependent attenuation of the drifting hot electrons which reach the probe tip having completed a minimum of three quarters of a drift orbit, with possible additional contributions from those which complete $N + \frac{3}{4}$ drift orbits where $N \geq 1$.

(iii) The distance between the observed peak locations should be $2h$, i.e. the diameter of the circular drift orbit which is determined by the height of the filament axis above the mirror axis.

(iv) A local minimum in the hot electron density would be expected, on symmetry grounds, at or close to the location on the probe path directly under the filament at $y = y_0$.

(v) For the alternative 'negative' orientation, labelled '**N**' in the next section, when **B** is oriented in the negative z direction (out of the page in figure 1(a)), the drift direction is reversed and hot electrons should drift anti-clockwise with reference to figure 1(a), and hence the stronger hot electron density peak should be located at $y = y_0 + h$ and the weaker at $y = y_0 - h$ along the probe path.

(vi) On symmetry grounds we would expect the amplitudes of the stronger and weaker peaks in the negative (**N**) orientation to be the same as those of the positive orientation (with locations exchanged).

Finally, since cold electrons result from inelastic collisions by the primary electrons, they should possess characteristics similar to those of the hot population, but modified by differences in collisionality and spatial distribution.

The foregoing calculations and predictions are relevant provided the bounce and drift timescales are shorter than the particle confinement time τ_p. The *a priori* calculation of mirror confinement times based on velocity space diffusion is challenging in this experiment since 0.1 eV nitrogen ion gyro radii in the symmetry plane range from 2 cm on axis to 4 cm at $r = 12.5$ cm and hence ions do not satisfy the magnetized plasma condition $\rho_{gyro}/D \ll 1$ where $D = 12.5$ cm is the relevant dimension of the plasma. Hence, depending on experimental conditions, electrons can be better confined than ions, and this is in fact observed in spatial profiles of the plasma potential reported below which can be both positive and negative. In the next section, analysis of density profiles derived from Langmuir probe data yields estimates of the global particle confinement time τ_p which confirm that this criterion is satisfied for the hot electron population where $\mathrm{T}_{orbit} \ll \tau_p$ but not for cold electrons where $\mathrm{T}_{orbit} > \tau_p$.

4. Experimental results

Langmuir probe traces with fitted parameters illustrative of low, medium and high pressure conditions in the results presented in this section are shown in figure 2(a-c). The low fit errors (rmse $< 0.5\%$ of maximum probe current) is evidence that the bi-Maxwellian model [10] used to fit the data gives credible values for the temperatures and (to within a fixed correction factor due to uncertainties in the effective probe collecting area) densities of the hot and cold electron populations. For the lowest pressure at which stable plasmas could be maintained, namely P = 0.2 mtorr, the hot electron temperature is maximum, and a fitted value of 40.1 eV was obtained for the probe trace in figure 2(a) where the floating potential-plasma potential difference is -76.3 V. By contrast, no

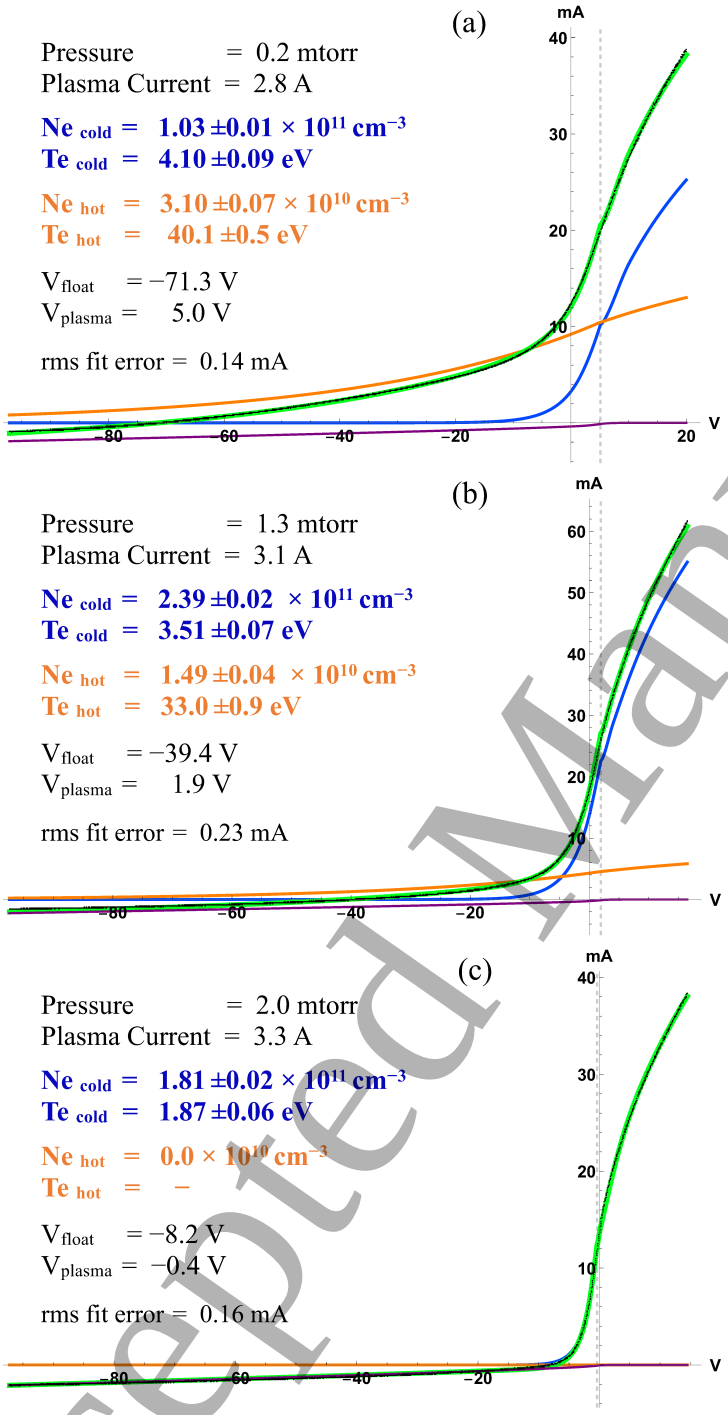

Figure 2. Raw (black dots) and fitted (green curve) Langmuir probe I(V) characteristics for (a) P=0.2 mtorr, (b) P=1.3 mtorr and (c) P=2.0 mtorr taken with the probe tip located (a) 220 mm, (b) 230 mm and (c) 80 mm from the baseplate. The blue, orange and purple curves are fitted cold electron, hot electron and ion contributions to the fitted I(V) characteristic. The vertical dashed line marks the location of the plasma potential. Parameter values are tabulated in each panel. See text for remarks on error bars.

fast electrons were present in the probe trace in figure 2(c) where the fitted electron temperature was 1.87 eV and $V_f - V_p$ was almost an order of magnitude lower at -7.8 V.

Traces similar to those in figure 2 were acquired for spatial scans at 10 mm intervals over the 300 mm range of the scanning probe system for 11 nitrogen pressures in the range 0.2 mtorr $\leq$ P $\leq$ 4 mtorr. In all cases the bias voltage varied from -90 V to -60 V across the incandescent filament windings, resulting in mean primary electron energies of $\simeq$ 75 eV. The heating circuit power was fixed at 560 W which resulted in plasma currents in the range 2.5 A $< I_p <$ 4.0 A. Each stored Langmuir $I(V)$ trace at a given spatial location is the average of 50 successive traces. A typical single trace consists of data taken over the voltage range $-100 < V < 25$ V at intervals of 0.05 V. Each point within a trace is sampled 30 times, so the stored, time-averaged traces each represent an average of 1500 samples. The natural scatter of the stored traces was empirically found to vary from $\approx 25\,\mu$A for $V < -30$ V to a maximum of $\approx 75\,\mu$A for $20 <$ V < 25 V.

In each case, spatial scans were taken for both orientations of the magnet stacks as described in section 3 ('**S**', the 'positive' orientation corresponding to **B** directed into the page in figure 1(a), and '**N**', the 'negative' orientation with **B** out the page). Figure 3 shows (for both magnetic orientations) spatial profiles of hot and cold electron densities and temperatures as well as floating and plasma potentials for the pressures specified on the density plots in the left column. The nominal range is $0 \leq y \leq 300$ mm but note that at $y = 0$ the centre of the 6 mm-long probe tip is 15 mm in from the baseplate surface.

In the **S** orientation, if the expected ring current behaviour is to be observed in the experiment, the near peak should correspond to hot electrons which have completed the shorter drift orbit path of $N + \frac{1}{4}$ orbits, $N \geq 0$, and the far peak should correspond to the longer path of $N + \frac{3}{4}$ drift orbits. For ease of reference this arrangement of the two peaks is termed near:$\frac{1}{4}$, far:$\frac{3}{4}$ or 'n:$\frac{1}{4}$, f:$\frac{3}{4}$' . For the negative (**N**) orientation of the two magnet stacks, the drift direction is reversed and the shorter drift path is to the far peak. Hence this arrangement is referred to as 'n:$\frac{3}{4}$, f:$\frac{1}{4}$'. The trends in the profiles presented in figure 3 for three of the 11 pressures are present in the full set of data for which peak hot electron densities versus pressure are plotted in figure 4. These findings can be itemized as follows:

(i) For all 11 pressures for which spatial scans were acquired, the dominant hot electron peak in the **S**/positive orientation is the near peak and the weaker peak is the far peak. This is consistent with the ring current n:$\frac{1}{4}$, f:$\frac{3}{4}$ arrangement.

(ii) In all cases the dominant hot electron peak in the **N**/negative orientation is the far peak and the weaker peak is the near peak. This, too, is consistent with the ring current n:$\frac{3}{4}$, f:$\frac{1}{4}$ arrangement.

(iii) The mean value and standard deviation of the location of the near hot electron peak as determined from the spline fit to each discrete profile of 31 spatial points is $\langle y_{near\,peak} \rangle = 119 \pm 1.6$ mm and, for profiles where the far peak is observable, $\langle y_{far\,peak} \rangle = 225 \pm 3.1$ mm. The separation of the peaks is 106 ± 4 mm consistent with a circular drift orbit of radius 50 mm (the height of the filament axis above the

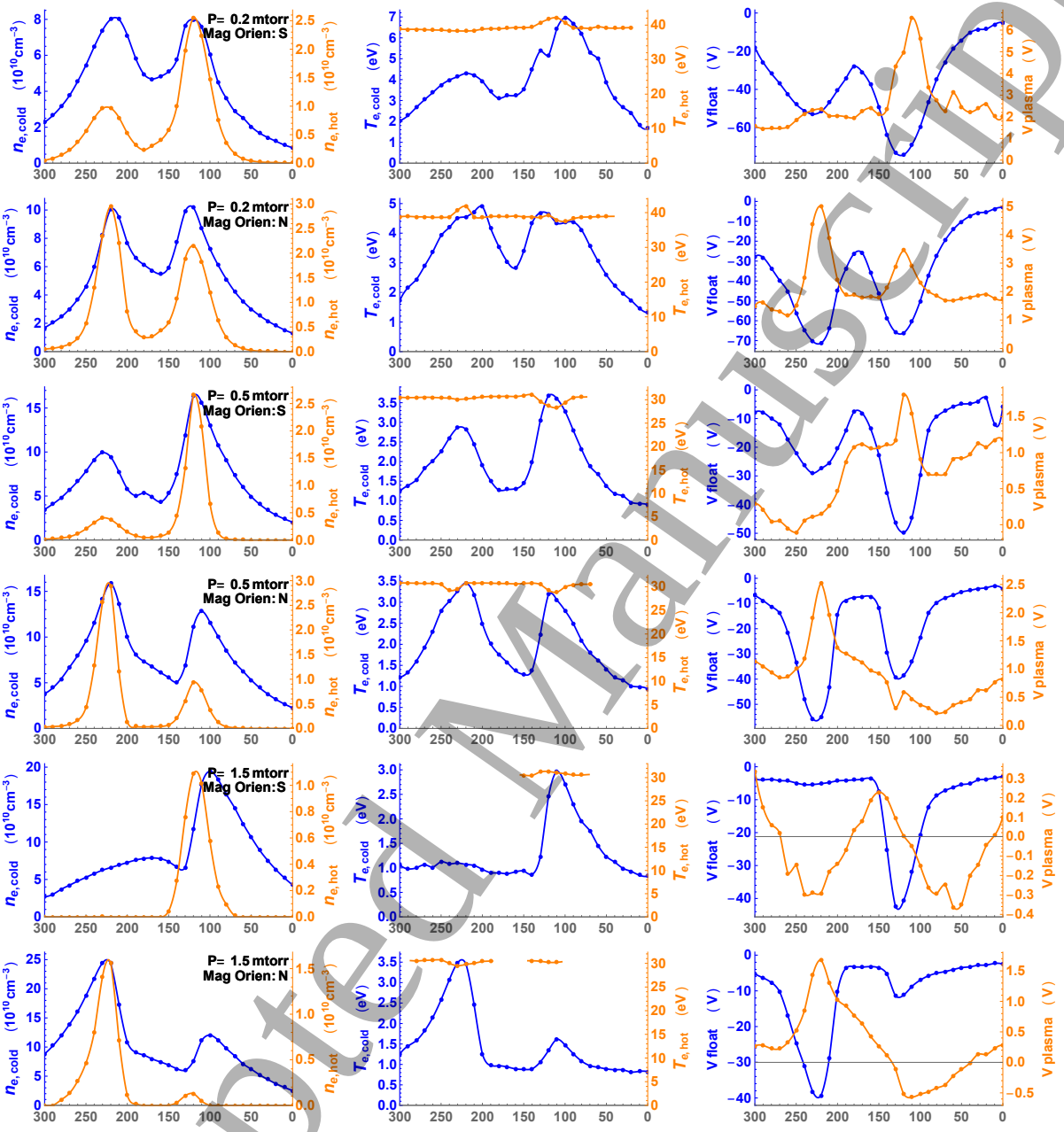

Figure 3. Spatial profiles along the probe path versus distance (mm) from the vessel baseplate of cold and hot electron densities (left column), cold and hot electron temperatures (middle column) and floating and plasma potentials (right column) from Langmuir probe spatial scans for $P = 0.2, 0.5, 1.5$ mtorr. The solid curves are cubic spline interpolations of the fitted parameters. Horizontal axes run from right to left to conform to the view of the vessel in figure 1(a) where the origin of the probe trajectory is at the baseplate to the right. $\mathrm{Te_{hot}}$ values are omitted when $\mathrm{Ne_{hot}} < 10^8\,\mathrm{cm}^{-3}$. For each pressure, profiles for both **S** and **N** orientations of the magnet stacks are presented. In all cases the bias voltage varied from -90 V to -60 V across the incandescent filament windings.

horizontal midplane of the vessel). By contrast, the separation of the cold electron peaks increases steadily with pressure from $\approx 95\,\mathrm{mm}$ to $\approx 130\,\mathrm{mm}$, a difference in which the higher collision frequency of cold electrons ($\propto T_e^{-3/2}$) is likely to play a role and which would in any case require transport modelling to explain quantitatively.

(iv) With increasing pressure, the ratio of the two peak amplitudes increases strongly, consistent with increased attenuation of the hot electron ring current caused by the extra semicircular drift path to be completed before the hot electrons first reach the location of the n:$\frac{3}{4}$ or f:$\frac{3}{4}$ peaks. For $p \geq 2\,\mathrm{mtorr}$, only the n:$\frac{1}{4}$ and f:$\frac{1}{4}$ hot electron peaks are present.

(v) A local minimum in the hot electron density, when both peaks are present, occurs in the range $170 \leq y \leq 180\,\mathrm{mm}$ which is close to or at the symmetric value of $\approx 172\,\mathrm{mm}$.

(vi) For each pressure, the disparity between the two peak amplitudes in the **S** orientation is more pronounced than in the **N** orientation. In the case of $P = 1.5\,\mathrm{mtorr}$ (see figure 3), there is no observable f:$\frac{3}{4}$ peak whereas the n:$\frac{3}{4}$ peak is present in the **N** orientation. The more pronounced disparity in the peak amplitudes for the **S** orientation is readily explained by the disruptive effect of the probe shaft on the ring current. The drift direction is clockwise in the **S** orientation and hot electrons reach the probe tip at the location of the near (n:$\frac{1}{4}$) peak without encountering the probe shaft. However, there is a significant probability of hot electrons colliding with the probe shaft before they reach the location of the far peak; hence the f:$\frac{3}{4}$ peak will be attenuated both by the longer drift path and by the presence of the probe shaft. The drift direction is anticlockwise in the **N** orientation and in this case the ring current reaches the probe tip at the location of the n:$\frac{3}{4}$ peak unimpeded by the probe shaft. In the case of the far peak the first pass, one-quarter-drift orbit contribution to the f:$\frac{1}{4}$ peak also reaches the probe tip unimpeded by the probe shaft, and while the current from hot electrons which complete $N + \frac{1}{4}$, $N > 0$ drift orbits is diminished by the presence of the shaft, its contribution to the f:$\frac{1}{4}$ peak amplitude, even with the effect of the probe shaft excluded, decreases rapidly with increasing pressure.

(vii) Finally, we note from equation 9 that for typical hot electron temperatures of 30 eV the ratio of electron to ion drift velocity for the reference ion temperature of 0.1 eV is $\approx$300 and hence the ring current is carried essentially exclusively by electrons.

4.1. Test for exponential attenuation of hot electron density

The hot electron ring current is attenuated along its drift orbit, where the azimuthal angle ϕ satisfies $\phi(t) = v_{dr}\,t/r_{ring} \propto t$ for fixed $r_{ring} \approx 50\,\mathrm{mm}$ and hence fixed v_{dr}, and t is the elapsed time since the hot electrons were emitted from the filament at $\phi = 0$. Elapsed time is also proportional to the total distance travelled following thermionic emission given by $s(t) \approx v_{th}\,t$ where $v_{th} = \sqrt{\mathrm{T_{e,\,hot}/m_e}}$ is the thermal

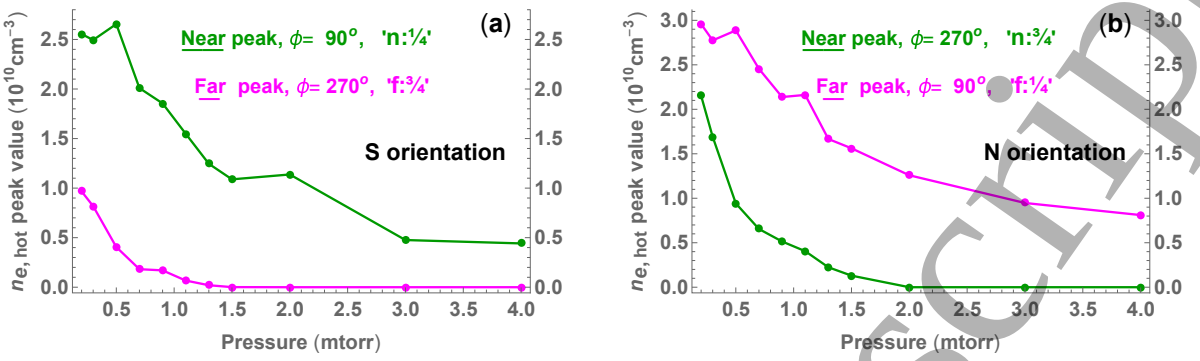

Figure 4. Hot electron density peak values versus gas pressure for (a) **S** and (b) **N** orientations for the full set of pressures for which spatial scans were acquired.

speed. Note that $s(t)$ includes both the more rapid bounce motion and still more rapid gyromotion and hence greatly exceeds the azimuthal drift distance $r\phi(t)$. Hence exponential attenuation of the hot electron density with distance travelled is expected, due principally to inelastic collisions with gas molecules and characterized by a mean free path $\lambda = 1/n\sigma \propto 1/p$ where σ is the cross-section and p is the gas pressure, provided the inelastic cross-section is approximately fixed for the experimental $\mathrm{T_{e,\,hot}}$ range. For inelastic electron collisions with nitrogen molecules, the cross-section in the energy range $25\,\mathrm{eV} < E_e < 120\,\mathrm{eV}$, equivalent to a temperature range $16\,\mathrm{eV} < \mathrm{T_e} < 80\,\mathrm{eV}$ which includes the experimental range of hot electron temperatures, lies in the narrow range $\sigma_{inelastic}(E_e) = 3.3 \pm 0.2 \times 10^{-16}\,\mathrm{cm}^2$, a result obtained from elastic and total scattering cross-section data in reference [15].

The hypothesis of exponential attenuation with $\lambda \propto 1/p$ can be tested using the ratio of the two peaks in the **N** orientation where the attenuation of the far f:$\frac{1}{4}$ peak due to the perturbing influence of the probe shaft, if present, is expected to be restricted to low pressures (see finding (vi) earlier in this section). If the beam attenuation is expressed in terms of ϕ, then

$$\begin{aligned} n_{\mathrm{e,\,hot}}(\phi) &= n_{\mathrm{e,\,hot}}(0)e^{-\delta\phi/\lambda} \\ &\equiv n_{\mathrm{e,\,hot}}(0)e^{-\phi p/\ell} \end{aligned} \tag{11}$$

where δ is the distance travelled per radian of azimuthal drift, $n_{\mathrm{e,\,hot}}(0)$ is the hot electron density when first leaving the filament and $\ell = \lambda p/\delta$ where ℓ is in units of mtorr. The ratio of the two peaks, ϱ, is then given by

$$\begin{aligned} \varrho \equiv \mathrm{f}:\tfrac{1}{4}/\mathrm{n}:\tfrac{3}{4} &= n_{\mathrm{e,\,hot}}(0)e^{-(\pi/2)p/\ell}/n_{\mathrm{e,\,hot}}(0)e^{-(3\pi/2)p/\ell} \\ &= \mathrm{e}^{\pi p/\ell} \end{aligned} \tag{12}$$

Accordingly, if exponential attenuation with a decay length inversely proportional to pressure correctly describes the peak ratio behaviour, the quantity $\ell = \pi p/\ln(\varrho)$ should be a constant independent of pressure. Figure 5 shows the peak ratio $\varrho = \mathrm{f}:\frac{1}{4}/\mathrm{n}:\frac{3}{4}$ and $\pi p/\ln(\varrho)$ for 8 of the 11 pressures for which the n:$\frac{3}{4}$ peak was present, namely for $0.2\,\mathrm{mtorr} \le \mathrm{p} \le 1.5\,\mathrm{mtorr}$. The horizontal dotted line marks the mean value of 1.87 mtorr

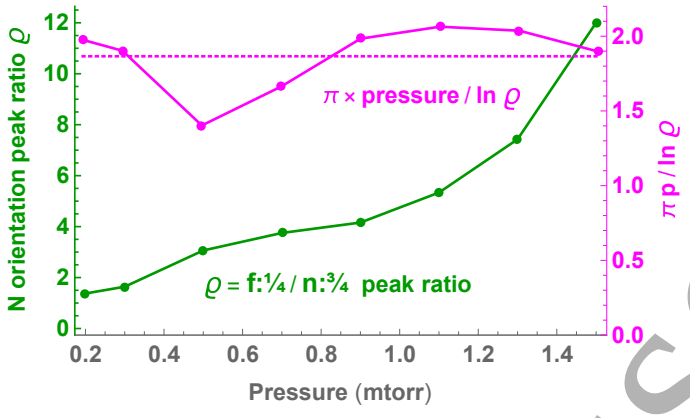

Figure 5. N orientation hot electron density peaks ratio ϱ (green trace) and $\pi p/\ln\varrho$ (magenta trace) versus nitrogen gas pressure for the 8 pressures for which both peaks were present. The horizontal dotted line marks the average value of 1.87 mtorr for the parameter $\ell = \pi p/\ln\varrho$.

with an associated standard deviation of 0.22. The lack of a systematic pressure-dependent pattern in the calculated values of ℓ and the modest $\pm 12\%$ standard deviation indicates that exponential attenuation with a mean free path inversely proportional to pressure is a good description of the dependence of the hot electron density on distance travelled.

4.2. Estimation of the particle confinement time τ_p

Density profiles acquired along the path of the movable probe which traverses the mirror symmetry plane can be used to make an estimate of the particle confinement time provided the total electron density profile $n_e(z)$ along the direction parallel to the mirror axis is known. Spatial scans made close to the mirror axis in helium plasmas using an older movable probe geometry which operated through a mid-vessel port (see figure 1(a)) resulted in density profiles obeying an approximate parabolic dependence: $n_e(z) = n_0(1 - z^2/z^2_{wall})$ for flux surfaces near the mirror axis with $n_e = n_0$ in the symmetry plane where $z = 0$.

The starting point in calculating the integral of $n_e(r, \phi, z)$ over the mirror volume is the area integral $\int n_e(r, \phi, 0)\, dA$ over the symmetry plane where $z = 0$. This yields dN/dz, the number of electrons per unit length in the axial direction at the symmetry plane. Note from figure 3 that the near and far portions of the cold electron density profiles are of comparable magnitude at all pressures, in contrast to the hot electrons where the n:$\frac{3}{4}$ and f:$\frac{3}{4}$ peaks become much weaker relative to the n:$\frac{1}{4}$ and f:$\frac{1}{4}$ peaks, ultimately disappearing (see figure 4) with increasing pressure. Hence separate approaches are needed for the hot and cold electron populations. The cold electron density at location y along the perturbation-free half of the trajectory on the near side of the filament is used as a representative value for $n_{\mathrm{e,\,cold}}(r(y), \phi, 0)$ where $0 \le \phi \le \pi$ in the case of the **S** orientation, and $\pi \le \phi \le 2\pi$ in the case of the **N** orientation. Here, $r(y) = y_0 - y$ is the radius of the flux surface in the symmetry plane at the location

y along the probe path. This approach enables the calculation of the number of cold electrons per unit length in the symmetry plane, where care must be taken to restrict the ϕ range when $r(y)$ exceeds the cylindrical radius of the vacuum vessel $R = 12.5\,\mathrm{cm}$:

$$\begin{aligned}\left(\frac{dN_{\mathrm{cold}}}{dz}\right)_{z=0} &= \int_{\substack{symm.\\plane}} n_{\mathrm{e,\,cold}}(r,\phi,0)\,dA \\ &\approx \int_{y=0}^{y_0} \left(n_{\mathrm{e,\,cold}}(y)_{\mathbf{S}} + n_{\mathrm{e,\,cold}}(y)_{\mathbf{N}}\right)\Delta\phi\, r(y)\,dy, \qquad (13)\end{aligned}$$

$$\Delta\phi = \begin{cases} \pi, & r(y) \le R \\ 2\arcsin(R/r(y)), & r(y) > R \end{cases}$$

The equivalent calculation for the hot electron density assumes exponential attenuation as calculated in the previous subsection. Thus $n_{\mathrm{e,\,hot}}(r,\phi,0) = n_{\mathrm{e,\,hot}}(r,0,0)\,e^{-\phi p/\ell}$ where $n_{\mathrm{e,\,hot}}(r(y),0,0) = n_{\mathrm{e,\,hot}}(y)_{\mathbf{S}}\,e^{+\pi p/2\ell}$ as is easily seen from equation (11). This gives:

$$\begin{aligned}\left(\frac{dN_{\mathrm{hot}}}{dz}\right)_{z=0} &= \int_{\substack{symm.\\plane}} n_{\mathrm{e,\,hot}}(r,\phi,0)\,dA \\ &\approx \int_{y=0}^{y_0}\int_{\phi=0}^{2\pi} n_{\mathrm{e,\,hot}}(y)_{\mathbf{S}}\,e^{+\pi p/2\ell}\,e^{-\phi p/\ell}\,d\phi\,r(y)\,dy \\ &= \frac{\ell}{p}e^{\pi p/2\ell}\left(1-e^{-2\pi p/\ell}\right)\int_{y=0}^{y_0} n_{\mathrm{e,\,hot}}(y)_{\mathbf{S}}\,r(y)\,dy \qquad (14)\end{aligned}$$

where here it is not neccessary to restrict the ϕ range since $n_{\mathrm{e,\,hot}} \approx 0$ for $r(y) \ge 12.5\,\mathrm{cm}$. The use of the same attenuation function $e^{-\phi p/\ell}$ for all $r(y)$ is justified by the approximate radial independence of the drift orbit period T_{dr} (see equations (8,9)) and hence the total distance travelled $s(t)$ is also approximately independent of drift orbit radius.

The integrals in equations (13) and (14) (the latter using $\ell = 1.87$, see figure 5) were evaluated for each pressure to yield dN/dz in the symmetry plane for cold and hot electrons. The empirically observed approximate parabolic dependence on z of $n_e(z)$ close to the mirror axis was assumed to hold everywhere, so that $n_e(r,\phi,z) = n_e(r,\phi,0)(1 - z^2/z_{wall}^2)$ for arbitrary r,ϕ,z which results in a simple proportionality between dN/dz at $z = 0$ and the total number of electrons:

$$\begin{aligned}N &= \int \frac{dN}{dz}\,dz \\ &= \int_{z=-R}^{R}\left(\frac{dN}{dz}\right)_{z=0}(1-(z/R)^2)\,dz \\ &= \left(\frac{dN}{dz}\right)_{z=0}\times\frac{4R}{3} \qquad (15)\end{aligned}$$

Figure 6(a) shows N for cold and hot electron populations (and their sum) versus pressure calculated using equations (13-15). Figure 6(b) shows the drift orbit period T_{dr} (in μs) calculated from equation (9) using the volume averaged electron temperature $\langle T\rangle = \int n_e T_e\,dV / \int n_e\,dV$ for cold and hot electrons, respectively. Also plotted is the particle confinement time (in μs) $\tau_P = N/\dot{N}$ where $\dot{N} = I_p/e$ for plasma current I_p and

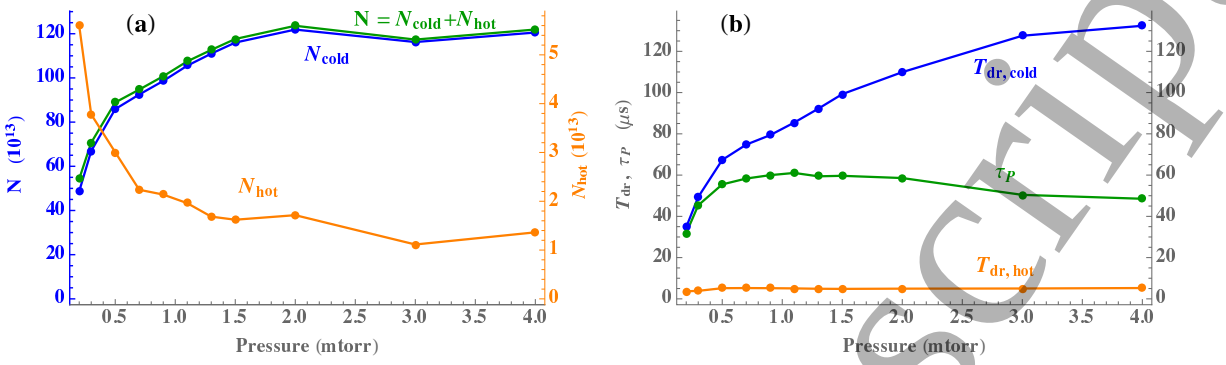

Figure 6. (a): Cold (blue trace), hot (orange trace) and total (green trace) number of electrons confined in the magnetic mirror versus nitrogen gas pressure; (b): Drift orbit period T_{dr} for cold (blue trace) and hot (orange trace) electrons and the particle confinement time τ_P (green trace). All times are in μs.

elementary charge e. For $p \geq 0.5\,\text{mtorr}$, τ_P lies ion the narrow range $50 \leq \tau_P \leq 60\,\mu\text{s}$. The hot electron drift period satisfies $T_{dr,\,hot}/\tau_P \approx 0.1$, thus fulfilling the criterion outlined at the end of section 3 for the relevance of the bounce and drift timescale calculations. This is not the case for the cold electrons where the drift period lies in the range $\tau_P < T_{dr,\,cold} < 3\tau_P$.

5. Discussion and conclusions

The shape of the plasma potential profile $V_{pl}(y)$ (see figure 3) usually closely tracks the hot electron density in the vicinity of the density peaks and hence has a positive maximum at the location of the hot electron density peak value. This gives rise to a radial electric field $\mathbf{E}_{rad} = -\nabla V_{pl}$ which is zero-valued at the peak density location and reaches oppositely directed extreme values at extrema in ∇V_{pl} which lie in the range $50 < |\mathbf{E}_{rad,\,max}| < 150\,\text{V/m}$. This radial electric field makes an additional contribution to the azimuthal drift. Its typical extreme value for $\text{B} \simeq 5\,\text{mT}$ near $r = r_{ring}$ is given by

$$\begin{aligned}(v_{dr,\,\mathbf{E}\times\mathbf{B}})_{max} &= |E_{rad,\,max}/B| \\ &\approx 100\,\text{V}\,\text{m}^{-1}/0.005\text{T} \\ &= 2\times 10^4\,\text{m}\,\text{s}^{-1}\end{aligned} \tag{16}$$

Evaluation of the combined $\nabla_\perp B$ and curvature drift (which, to distinguish it from the total drift, we now label $v_{dr,\,\nabla_\perp B}$) for a typical hot electron temperature of 30 eV at the filament radius $r = r_{ring} = 50\,\text{mm}$ using equation (9) yields a value of $6.28\times 10^4\,\text{m}\,\text{s}^{-1}$ and we conclude that the $\mathbf{E}\times\mathbf{B}$ drift makes a significant but limited contribution to the overall hot electron drift. Moreover, the ratio of drift to thermal velocity at $r = r_{ring}$ is $\approx 0.005\sqrt{T_e}$ (for T_e in eV) and hence electron drift plays a negligible role in the interpretation of probe data.

To quantify the localized effect of the $\mathbf{E}\times\mathbf{B}$ drift for the electrons, we consider first the region along the probe path between the peaks, i.e. for $r(y) < r_{ring}$ where

(see figure 3) $\nabla V_{pl} = \partial V_{pl}(r)/\partial r > 0$ and hence $E_{rad} = -\nabla V_{pl}$ is directed radially inwards. Here, the $\mathbf{E} \times \mathbf{B}$ drift is clockwise for the **S** orientation and anticlockwise for the **N** orientation, which in both cases is in the same direction as $v_{dr,\nabla_\perp B}$ and hence leads to an increased net v_{dr}. For $r(y) > r_{ring}$, $\partial V_{pl}(r)/\partial r < 0$ and hence the $\mathbf{E} \times \mathbf{B}$ drift is oppositely directed to $v_{dr,\nabla_\perp B}$ leading to a weakened net v_{dr}. But a reduced net drift velocity results in a longer drift orbit period and hence a greater value of $s(t)$, the total distance travelled by drifting electrons which have orbited through a given azimuthal distance. This implies a greater attenuation of the hot electron density on the $r(y) > r_{ring}$ side of the peak and a reduced attenuation on the $r(y) < r_{ring}$ side. Where asymmetries in the hot electron density peak shape are visible, in particular for the $p = 1.5\,\mathrm{mtorr}$ profiles in figure 3, the effect, however, appears to be opposite to that expected, since the hot electron density profiles decay more steeply on the $r(y) < r_{ring}$ side (i.e. on the mirror axis side) of the peak locations.

In contrast to electrons, the $\mathbf{E} \times \mathbf{B}$ drift, which is identical for all plasma species, would appear to have dramatic consequences for the ion current to the probe, since ionized nitrogen molecules travelling at $2 \times 10^4\,\mathrm{m\,s^{-1}}$ satisfy $\frac{1}{2}Mv^2 = 58\,\mathrm{eV}$. A condition for the validity of particle drift expressions is that the gyroradius be much smaller than relevant scale lengths. The scale length for ∇V_{pl} is given by $L_{E_{rad}} \approx 20\,\mathrm{mm}$ and, for 30 eV electrons in a magnetic field of 5.2 mT, the gyroradius $\rho_g = 2.5\,\mathrm{mm}$ yields a small finite Larmor radius parameter $\epsilon = \rho_g/L \approx 0.125$. For $T_i = 0.1\,\mathrm{eV}$ ions, however, $\rho_g = 33\,\mathrm{mm}$ and $\epsilon > 1$ so that the drift condition is strongly violated, and in fact ion gyromotion is large enough to span both positive and negative $\partial V_{pl}(r)/\partial r$ regions in a single gyro-orbit which would indicate a substantial reduction in, if not effective elimination of, directed ion motion. The complex calculations to correctly model these conditions lie outside the scope of this work.

Finally, we remark that in figure 4, the f:$\frac{1}{4}$ peak is moderately and systematically stronger than the n:$\frac{1}{4}$ peak when the inequality, at least for very low pressures, would be expected in the other direction due to the perturbing influence of the probe shaft. One possible explanation for this discrepancy would be a left/right asymmetry (with reference to figure 1(a)) in the efficiency of the filament surface causing a somewhat stronger electron fluence away from the baseplate. This would result in a small anticlockwise shift in the zero position of the azimuthal angle ϕ, thus enhancing the f:$\frac{1}{4}$ peak relative to the n:$\frac{1}{4}$. Another possible reason for the stronger f:$\frac{1}{4}$ peak is the fact that the mirror axis is 185 mm distant from the baseplate as against 285 mm from the other end of the cylindrical vessel, a necessary asymmetry due to the limited scan range of the probe. The closer proximity of the baseplate where the electron density is clamped at zero could explain the imbalance in the peak strengths, however appropriate modelling calculations would be required to test this hypothesis.

In summary, the experimental results presented here show clear signatures of a ring current of primary electrons emitted from a hot filament located within an axisymmetric magnetic mirror configuration. Analyses of spatial Langmuir probe scans using a bi-Maxwellian fitting model yield hot electron density profiles with localized peaks of

unequal strengths at locations along the probe path consistent with intersection by a circular ring current whose radius is given by the height of the hot filament above the scan path. The locations of the stronger and weaker peaks are exchanged when the orientation of the mirror field is reversed, a result which strongly supports the ring current hypothesis. The dependence of the ratio of the two peak amplitudes on gas pressure p is consistent with exponential attenuation of the hot electron density along the drift orbit with a mean free path $\lambda_{mfp} \propto 1/p$. Finally, an estimate of the total number of electrons in the mirror volume yielded a particle confinement time in the range $50 \leq \tau_P \leq 60\,\mu$s for $0.5 \leq p \leq 4\,$mtorr.

6. Acknowledgements

The first author warmly acknowledges the assistance and advice of Richard Armstrong over many years and his key role in bringing the experimental apparatus to UCC. The generosity of Bill Graham in arranging a permanent loan of the then Double Plasma experiment from Queen's University Belfast to University College Cork is likewise acknowledged. This work has been carried out within the framework of the EUROfusion Consortium in the context of the PhD project of the second author and has received funding from the Euratom research and training programme 2014-2018 under grant agreement number 633053. The views and opinions expressed herein do not necessarily reflect those of the European Commission.

7. References

[1] Gonzales W D et al., J. Geophys. Res. **99** (1994) 5571.
[2] Daglis I A et al., Rev. Geophys. **37** (1999) 407.
[3] Chapman S and Ferraro V C A, Terrest. Magnetism and Atmospheric Elec., **36** (1931) 77, 171.
[4] Sonett C P at al., Phys. Rev. Lett. **4** (1960) 161.
[5] Furukawa T at al., Phys. Plas. **26** 033505 (2019).
[6] Takahashi K et al., Plasma Sources Sci. Technol. **25** 055011 (2016).
[7] Ghosh S et al., Phys. Plas. **24** 020703 (2017).
[8] Godyak V A and Demidov V I, J. Phys. D-Appl. Phys. **44** 233001 (2011).
[9] Daglis I A, Space Sci. Rev. **124** (2006) 183.
[10] Mc Carthy P J, Cahill B, Morgan T J, Armstrong R A, *Comparison of probe and spectroscopic data in a $T_e \geq 10\,eV$ magnetic mirror laboratory plasma.* 30th ICPIG, Belfast, 28th Aug. - 2nd Sep. 2011.
[11] Chung CW, Kim S S, Yang, H Y, Phys. Rev. Lett. **88** 095002 (2002).
[12] Derby N and Olbert S, Am. J. Phys. **78** (2010) 229.
[13] Goldston R J and Rutherford P H 1995 *Introduction to Plasma Physics* (Bristol and Philadelphia: IOP Publishing).
[14] Knott S et al. (in preparation).
[15] Itikawa Y, J. Phys. Chem. Ref. Data **35** (2006) 31.